HHS Public Access

Author manuscript

Brain Pathol. Author manuscript; available in PMC 2021 January 01.

Published in final edited form as:

Brain Pathol. 2020 January ; 30(1): 46–62. doi:10.1111/bpa.12747.

High-grade neuroepithelial tumor with *BCOR* exon 15 internal tandem duplication – a comprehensive clinical, radiographic, pathologic, and genomic analysis

Sean P. Ferris[1], **Jose Velazquez Vega**[2], **Mariam Aboian**[3], **Julieann C. Lee**[1], **Jessica Van Ziffle**[1,4], **Courtney Onodera**[1,4], **James P. Grenert**[1,4], **Tara Saunders**[1], **Yunn-Yi Chen**[1], **Anu Banerjee**[5], **Cassie N. Kline**[5,6], **Nalin Gupta**[7], **Corey Raffel**[7], **David Samuel**[8], **Irune Ruiz-Diaz**[9], **Shino Magaki**[10], **Dianne Wilson**[11], **Janna Neltner**[11], **Zahra Al-Hajri**[12], **Joanna J. Phillips**[1,7], **Melike Pekmezci**[1], **Andrew W. Bollen**[1], **Tarik Tihan**[1], **Matthew Schniederjan**[2], **Soonmee Cha**[3], **Arie Perry**[1,7], **David A. Solomon**[1,4]

[1.]Department of Pathology, University of California, San Francisco, CA, United States

[2.]Department of Pathology, Children's Healthcare of Atlanta, Atlanta, GA, United States

[3.]Department of Radiology and Biomedical Imaging, University of California, San Francisco, CA, United States

[4.]Clinical Cancer Genomics Laboratory, University of California, San Francisco, CA, United States

[5.]Division of Pediatric Hematology/Oncology, Department of Pediatrics, University of California, San Francisco, CA, United States

[6.]Department of Neurology, University of California, San Francisco, CA, United States

[7.]Department of Neurological Surgery, University of California, San Francisco, CA, United States

[8.]Department of Hematology-Oncology, Valley Children’s Hospital, Madera, CA, United States

[9.]Department of Pathology, Hospital Universitario Donostia, Gipuzkoa, Spain

[10.]Department of Pathology and Human Anatomy, Loma Linda University Medical Center, Loma Linda, CA, United States

[11.]Department of Pathology and Laboratory Medicine, University of Kentucky, Lexington, KY, United States

[12.]Department of Histopathology, Khoula Hospital, Sultanate of Oman

To whom correspondence should be addressed: To whom correspondence should be addressed: David A. Solomon, MD, PhD, Division of Neuropathology, Department of Pathology, University of California, San Francisco, 513 Parnassus Ave, Health Sciences West 451, San Francisco, CA 94143, Phone (415) 514-9761, david.solomon@ucsf.edu.

Conflict of interest

None of the authors have any conflicts of interest to disclose.

Data Availability

Scanned image files of H&E stained sections from the ten tumors from which representative images are presented are available for downloading and viewing at the following link: https://figshare.com/projects/High-grade_neuroepithelial_tumor_with_BCOR_exon_15_internal_tandem_duplication/61691. Sequencing data files are available from the authors upon request.

Abstract

High-grade neuroepithelial tumor with *BCOR* exon 15 internal tandem duplication (HGNET *BCOR* ex15 ITD) is a recently proposed tumor entity of the central nervous system (CNS) with a distinct methylation profile and characteristic genetic alteration. The complete spectrum of histologic features, accompanying genetic alterations, clinical outcomes, and optimal treatment for this new tumor entity are largely unknown. Here, we performed a comprehensive assessment of ten new cases of HGNET *BCOR* ex15 ITD. The tumors mostly occurred in young children and were located in the cerebral or cerebellar hemispheres. On imaging all tumors were large, well-circumscribed, heterogeneous masses with variable enhancement and reduced diffusion. They were histologically characterized by predominantly solid growth, glioma-like fibrillarity, perivascular pseudorosettes, and palisading necrosis, but absence of microvascular proliferation. They demonstrated sparse to absent GFAP expression, no synaptophysin expression, variable OLIG2 and NeuN positivity, and diffuse strong BCOR nuclear positivity. While *BCOR* exon 15 internal tandem duplication was the solitary pathogenic alteration identified in six cases, four cases contained additional alterations including *CDKN2A/B* homozygous deletion, *TERT* amplification or promoter hotspot mutation, and damaging mutations in *TP53*, *BCORL1*, *EP300*, *SMARCA2*, and *STAG2*. While the limited clinical follow-up in prior reports had indicated a uniformly dismal prognosis for this tumor entity, this cohort includes multiple long-term survivors. Our study further supports inclusion of HGNET *BCOR* ex15 ITD as a distinct CNS tumor entity and expands the known clinicopathologic, radiographic, and genetic features.

INTRODUCTION

A recent genomic profiling study of tumors previously diagnosed as primitive neuroectodermal tumor of the central nervous system (CNS-PNET) identified a new subtype of high-grade neuroepithelial tumor unified by a recurrent internal tandem duplication within exon 15 of the *BCOR* transcriptional co-repressor gene and a distinct genome-wide methylation profile compared to all other CNS tumor entities assessed to date (26). These tumors (hereafter abbreviated HGNET *BCOR* ex15 ITD) predominantly arose in the cerebral or cerebellar hemispheres of young children, had an approximately equal male to female distribution, were histologically characterized by perivascular pseudorosettes and glioma-like fibrillarity, and had poor outcomes in the small number of cases with available clinical follow-up.

The protein product of the *BCOR* gene was initially identified in 2000 as a novel binding partner of BCL6, which is a POZ/zinc finger domain-containing transcriptional repressor protein (9). BCOR was demonstrated to function as a transcriptional co-repressor when tethered to DNA that potentiated BCL6 mediated repression, specifically through its association with class I and II histone deacetylases (9). Inherited/constitutional mutations in the *BCOR* gene were identified in 2004 as the cause of an X-linked oculofaciocardiodental syndrome (Online Mendelian Inheritance in Man #300166) characterized by microphthalmia, congenital cataracts, long narrow face, dental radiculomegaly with persistent primary teeth, and cardiac septal defects (15). Studies in osteodentinogenic mesenchymal stem cells from a patient with oculofaciocardiodental syndrome found that *BCOR* mutation disrupted homeostasis by resulting in increased methylation of lysine 4 and

lysine 36 on the tail of histone H3, thereby reactivating transcription of silenced target genes (6). Thus, *BCOR* appears to be a critical epigenetic regulatory gene whose constitutional disruption results in a severe developmental syndrome affecting multiple organ systems.

Whereas constitutional mutations in the *BCOR* gene perturb organogenesis during development, somatic alterations in *BCOR* have now been identified as recurrent genetic drivers in a wide spectrum of human tumor types. A recurrent internal tandem duplication within exon 15 of *BCOR* has been identified as the defining genetic alteration in clear cell sarcoma of the kidney, primitive myxoid mesenchymal tumor of infancy, and a subset of CNS high-grade neuroepithelial tumors (2, 10, 23, 26, 24, 28). Distinct from exon 15 internal tandem duplication, in-frame gene fusions involving the *BCOR* gene are present in a subset of endometrial stromal sarcomas, pediatric low-grade gliomas, and undifferentiated round cell sarcomas of bone and soft tissue, most often with the *ZC3H7B* gene in endometrial stromal sarcomas, the *EP300* gene in pediatric low-grade gliomas, and the *CCNB3* gene in bone and soft tissue sarcomas (13, 18, 20, 21, 25, 27). Lastly, somatic truncating mutations or homozygous deletions of *BCOR* have been recurrently found in acute myeloid leukemia, retinoblastoma, medulloblastoma, and diffuse gliomas (5, 8, 12, 14, 16, 22, 29). Thus, the *BCOR* gene appears to be an important oncogenic driver in a broad spectrum of human tumor types, with distinct genetic alterations specific to different tumor entities.

Only a few additional patients with HGNET *BCOR* ex15 ITD have been reported since the initial description of this tumor entity by Sturm *et al* (1, 19, 26, 30). As such, the full spectrum of histologic features, accompanying genetic alterations, clinical outcomes, and optimal treatment for this new tumor entity remain largely undefined. Here, we report our experience with the clinical, radiographic, histologic, ultrastructural, and genetic features of ten new cases of HGNET *BCOR* ex15 ITD.

METHODS

Patient cohort

Ten children diagnosed with high-grade neuroepithelial tumors found to harbor *BCOR* exon 15 internal tandem duplication by targeted next-generation sequencing analysis at UCSF Medical Center were included in this study. Patient SF-BCOR-2 has been previously reported in part (11). Pre-operative imaging studies were reviewed for each patient by two expert neuro-radiologists (M.A. and S.C.). This study was approved by the Committee on Human Research of the University of California, San Francisco, with a waiver of patient consent.

Tumor samples and histology review

All tumor specimens were fixed in 10% neutral-buffered formalin and embedded in paraffin. Pathologic review of all tumors was conducted by a group of expert neuropathologists (S.P.F., M.P., A.W.B., T.T., A.P., and D.A.S.).

Immunohistochemistry

Immunohistochemistry was performed on whole formalin-fixed, paraffin-embedded tissue sections using the following antibodies: glial fibrillary acidic protein (GFAP, Dako, cat# GA524, polyclonal, 1:3000 dilution, 15 min incubation); oligodendrocyte transcription factor 2 (OLIG2, Immuno Bio Labs, polyclonal, 1:200 dilution, 30 min incubation); NeuN (Chemicon, cat# MAB377, clone A60, 1:4000 dilution, 15 min incubation); synaptophysin (Cell Marque, cat# 336A, polyclonal, 1:100 dilution, 30 min incubation); neurofilament (Cell Marque, cat# 302M, clone 2F11, undiluted, 30 min incubation); epithelial membrane antigen (EMA, Leica, cat# PA0035, clone GP1.4, undiluted, 15 min incubation); BCOR (Santa Cruz Biotechnology, cat# sc-514576, clone C-10, 1:200 dilution, 30 min incubation); p53 (Leica, cat# PA0057, clone DO-7, undiluted, 15 min incubation); Ki67 (Dako, cat# GA626, clone MIB1, 1:50 dilution, 30 min incubation). All immunostaining was performed on a Leica Bond-III automated stainer. ER1 antigen retrieval was used for OLIG2, neurofilament, NeuN, and EMA antibodies. ER2 antigen retrieval was used for synaptophysin, BCOR, p53, and Ki67 antibodies. No antigen retrieval was performed for GFAP. Diaminobenzidine was used as the chromogen, followed by hematoxylin counterstain.

Electron microscopy

Ultrathin (80 nm) sections of glutaraldehyde-fixed, Epon-embedded tissue were stained with 2% uranyl acetate at the UCSF Electron Microscopy Core Lab. Sections were subsequently examined in a JEOL 1400 transmission electron microscope at 120 kV. Images were recorded with a Gatan SC1000 CCDE camera.

Targeted next-generation sequencing

Genomic DNA was extracted from formalin-fixed, paraffin-embedded blocks of tumor tissue from the ten tumors using the QIAamp DNA FFPE Tissue Kit (Qiagen). In nine cases, tumor tissue from the initial resection was used for sequencing analysis. The tumor tissue analyzed for patient SF-BCOR-8 was from the recurrent tumor following initial gross total resection, 60 Gy cranial radiation, and adjuvant chemotherapy with temozolomide and bevacizumab. Genomic DNA was also extracted from a peripheral blood sample for four patients (SF-BCOR-1, SF-BCOR-2, SF-BCOR-5, and SF-BCOR-7) using the QIAamp DNA Blood Midi Kit (Qiagen). Capture-based next-generation DNA sequencing was performed using an assay that targets all coding exons of 479 cancer-related genes, select introns and upstream regulatory regions of 47 genes to enable detection of structural variants including gene fusions, and DNA segments at regular intervals along each chromosome to enable genome-wide copy number and zygosity analysis, with a total sequencing footprint of 2.8 Mb (UCSF500 Cancer Panel; Supplementary Table 1; reference 11). Multiplex library preparation was performed using the KAPA Hyper Prep Kit (Roche) according to the manufacturer’s specifications using 250 ng of sample DNA. Hybrid capture of pooled libraries was performed using a custom oligonucleotide library (Nimblegen SeqCap EZ Choice). Captured libraries were sequenced as paired-end 100 bp reads on an Illumina HiSeq 2500 instrument. Sequence reads were mapped to the reference human genome build GRCh37 (hg19) using the Burrows-Wheeler aligner (BWA). Recalibration and deduplication

of reads was performed using the Genome Analysis Toolkit (GATK). Coverage and sequencing statistics were determined using Picard CalculateHsMetrics and Picard CollectInsertSizeMetrics. Single nucleotide variant and insertion/deletion mutation calling was performed with FreeBayes and PinDel. Structural variant calling was performed with Delly. Variant annotation was performed with Annovar. Single nucleotide variants and insertions/deletions were visualized and verified using Integrated Genome Viewer. Genome-wide copy number analysis based on on-target and off-target reads was performed by CNVkit and visualized using Nexus Copy Number (Biodiscovery).

Clinical summary and Kaplan-Meier survival analysis

Kaplan-Meier survival analysis was performed using GraphPad Prism software. In addition to the ten patients from this cohort, all previously reported cases of high-grade neuroepithelial tumors with confirmed *BCOR* exon 15 internal tandem duplication by targeted Sanger or next-generation sequencing were included in the clinical summary and survival analysis in Figure 10. These included 15 cases from Sturm *et al*, 6 cases from Yoshida *et al*, 3 cases from Appay *et al*, and 1 case from Paret *et al* (1, 19, 26, 30). The clinical features and data source of these previously reported 25 patients are shown in Supplementary Table 9. This analysis excluded the 19 cases from Sturm *et al* that clustered with “CNS high-grade neuroepithelial tumor with *BCOR* alteration” but did not have genetic analysis confirming *BCOR* exon 15 internal tandem duplication (26).

RESULTS

Clinical features

The three male and seven female patients ranged from 1–13 years old (median 3 years) at time of initial diagnosis (Table 1 and Supplementary Table 2). Seven tumors were in young children less than 5 years old, while three tumors were in older children. Presenting symptoms were variable ranging from headaches to seizures to focal neurologic deficits. Tumors were located in the cerebral hemispheres in five patients, in the cerebellar hemispheres in four patients, and in the basal ganglia in one patient. The cerebellar tumors were exclusively present in young children less than 5 years old, while the supratentorial tumors were present in both young and older children.

Imaging features

Pre-operative magnetic resonance imaging revealed solid, well-circumscribed masses in each of the ten patients (Figure 1 and Supplementary Table 3). The tumors were all large with associated mass effect. Maximal dimension ranged from 3.8 to 10.2 cm. Many of the tumors demonstrated central areas of necrosis or blood products. Contrast enhancement was variable but never showed the ring-enhancing pattern characteristic of most glioblastomas. Diffusion weighted imaging often showed reduced diffusion suggestive of high cellularity neoplasms. Most tumors abutted the overlying dura without definite invasion. No cerebrospinal dissemination was seen at time of diagnosis in any of the patients.

Histologic features

The ten tumors all demonstrated a predominantly solid growth pattern with a sharp border with adjacent brain parenchyma, although a couple of tumors showed infiltration at their interface with adjacent brain (Figures 2-4, Table 3, and Supplementary Table 4). A prominent feature uniformly seen in all tumors was ependymoma-like perivascular pseudorosettes with tumor cells aggregated around blood vessels with an intervening anuclear zone; however, in contrast to ependymoma, the perivascular processes were negative for GFAP (see below). The tumor cells were characterized by round to oval nuclei with fine chromatin. Most examples demonstrated glioma-like fibrillarity. Necrosis was observed in all tumors, almost always with palisading of the tumor cells at the periphery. All tumors were highly vascular with a rich branching capillary network. However, well-developed microvascular proliferation was not identified in any of the ten cases. Cellularity and mitotic activity was variable, ranging from areas with low cellularity and scant mitoses to densely cellular areas with numerous mitoses. Some of the tumors had a myxoid and microcystic background, while others had marked stromal and perivascular hyalinization reminiscent of astroblastoma. Microcalcifications were seen in a minority of cases. Rosenthal fibers and eosinophilic granular bodies were not observed in any of the tumors. Three cases featured distinctive Homer Wright-like rosettes, with tumor cells rosetted around central areas of eosinophilic fibrillar processes; this often raised a differential diagnostic consideration of medulloblastoma or other embryonal neoplasms. However, both the tumor cells and central cores of these rosettes lacked synaptophysin expression (see below), differentiating them from true Homer Wright (neuroblastic) rosettes.

Immunohistochemical features

Immunostaining for GFAP was negative in all or the vast majority of tumor cells in the nine evaluated cases (Figure 5 and Table 3). However, OLIG2 positivity was observed in most tumors, with variable labeling ranging from 10–40% of tumor cells. NeuN positivity was also observed in most tumors, with variable labeling of tumor nuclei ranging from 10–80%. Synaptophysin labeling was uniformly negative in the nine evaluated tumors. Immunohistochemistry for neurofilament protein often show scattered cells with cytoplasmic staining. Immunostaining for epithelial membrane antigen (EMA) was typically negative or showed faint granular cytoplasmic staining, distinct from the dot-like or ring-like staining pattern typically seen in ependymomas. Diffuse strong nuclear staining for BCOR protein was observed in the eight evaluated cases. The Ki-67 labeling index was variable ranging from 15–60% in the highest areas.

Ultrastructural features

Transmission electron microscopy was performed on two of the tumors (SF-BCOR-1 and SF-BCOR-7). This analysis showed primitive cells with abundant rough endoplasmic reticulum and limited intermediate cytoskeletal filaments (Figure 6). No tight junctions, cilia, or microvilli characteristic of ependymoma were seen. Additionally, no neurosecretory granules or synaptic vesicles were seen.

Targeted next-generation sequencing results

Targeted next-generation sequencing of approximately 500 cancer-associated genes and genome-wide copy number analysis was performed on the ten tumors as described in the Methods. A tandem duplication within exon 15 of the *BCOR* gene was identified in all ten cases (Figures 7-8, Supplementary Table 5). The minimally duplicated codons across all ten tumors were p.L1713_G1738 (RefSeq transcript NM_001123385).

In six cases, the *BCOR* exon 15 internal tandem duplication was the solitary pathogenic alteration identified. Four cases contained additional genetic alterations considered likely to be contributing to tumor pathogenesis (Supplementary Tables 6 and 7). These included SF-BCOR-9 with *TERT* promoter hotspot mutation and a splice site mutation in the *SMARCA2* chromatin remodeling gene. SF-BCOR-6 contained an additional truncating frameshift mutation in the *CREBBP* histone acetyltransferase gene, while SF-BCOR-10 contained a damaging missense mutation in the *TP53* tumor suppressor gene. The genomic profiling that was performed for patient SF-BCOR-8 was on the recurrent tumor following initial gross total resection, 60 Gy cranial radiation, and adjuvant chemotherapy with temozolomide and bevacizumab. This recurrent tumor SF-BCOR-8 harbored *BCOR* exon 15 internal tandem duplication along with additional *CDKN2A/B* homozygous deletion, *TERT* promoter hotspot mutation (c.−124C>T), two truncating frameshift mutations in the *BCORL1* gene, and a splice site mutation in the *STAG2* gene. Whether any of these alterations were present in the initial tumor versus acquired during disease progression after therapy is unknown.

The somatic mutation burden was uniformly very low (less than 2 somatic mutations per Mb within the 2.8 Mb of the tumor genome that was interrogated by the sequencing assay). Among the four patients in which a normal sample was also sequenced, no pathogenic germline alterations associated with increased cancer risk were identified.

Five of the tumors demonstrated a balanced diploid genome without chromosomal gains or losses (Supplementary Table 8). Three of the tumors demonstrated a paucity of chromosomal gains/losses (fewer than 4). Two of the tumors (SF-BCOR-9 and SF-BCOR-10) demonstrated markedly aneuploid genomes with numerous chromosomal gains and losses, both at time of initial resection in the absence of prior therapy. No recurrent chromosomal gains or losses in more than two of the ten tumors were observed.

Anaplastic features in HGNET *BCOR* exon 15 ITD

Case SF-BCOR-10 demonstrated two distinct histologic components (Figure 9). One was a lower grade appearing component with moderate cellularity, abundant fibrillarity, numerous calcifications, and scant mitoses. This was apposed to an overtly anaplastic component featuring dense cellularity, increased nuclear pleomorphism, and brisk mitotic activity. The anaplastic component was sharply demarcated from the lower grade component enabling genomic profiling to be performed separately on the two regions. Both components contained the identical *BCOR* exon 15 internal tandem duplication and a damaging missense mutation in the *TP53* tumor suppressor gene. The lower grade component had monosomy 13q as the solitary chromosomal copy number alteration, whereas the anaplastic component

harbored numerous chromosomal gains and losses (+1p, +1q [4N], +2, +6, +7, +12, +14q, +15q, +17, +18 [4N], +19, +21q [4N], and +22q).

Clinical outcomes

The complete clinical data including extent of resection, treatment regimen, and outcome data from the ten patients are presented in Table 1 and Supplementary Table 2. All ten patients initially underwent gross total resection. Four children were subsequently treated with cranial radiation, two children with craniospinal radiation with a boost to the tumor bed, and four children did not receive radiation as part of their immediate post-resection therapy. The initial chemotherapy regimen was temozolomide and bevacizumab following a high-grade glioma therapy protocol for three children, while six children were initially treated with an intensive multiagent chemotherapy regimen following an embryonal tumor therapy protocol. One child (SF-BCOR-4) did not receive any adjuvant radiation or chemotherapy following initial resection.

Clinical follow-up for this cohort of ten children ranged from 0.4 to 14.2 years (median 2.0 years). Four children experienced tumor recurrence at 4, 14, 31, and 49 months after initial resection. The earliest recurrence at 4 months was in the child who did not receive any adjuvant therapy (SF-BCOR-4), who later developed disseminated disease along the spinal cord at 20 months after initial diagnosis. Two of the other children who experienced recurrence at 31 and 49 months had been treated with cranial radiation and chemotherapy following a high-grade glioma therapy protocol with temozolomide and bevacizumab (SF-BCOR-8 and SF-BCOR-9). The fourth child who experienced recurrence at 14 months (SF-BCOR-1) had not received radiation therapy but was treated with platinum-based multiagent chemotherapy following an embryonal tumor therapy protocol. These four children all underwent a second resection confirming tumor recurrence, followed by additional radiation and/or chemotherapy. The recurrent disease in these four children was localized (adjacent to the prior resection cavity), with only one patient in this cohort later experiencing cerebrospinal dissemination (SF-BCOR-4). All of the ten children in this cohort were alive at last clinical follow-up, including two long-term survivors at 4.5 years (SF-BCOR-8) and 14.2 years (SF-BCOR-1) after initial diagnosis.

We next curated clinical data from all reported cases of CNS high-grade neuroepithelial tumor with confirmed *BCOR* exon 15 internal tandem duplication (Supplementary Table 9). Patient age, sex, tumor location, and survival data were analyzed from the 10 patients in our cohort together with these 25 previously reported patients (Figure 10). The median patient age was 3.5 years (range 0–22 years) at time of initial diagnosis. These 35 patients included 16 males and 19 females. Tumors were located in the cerebellar hemispheres (n=16), cerebral hemispheres (n=14), basal ganglia (n=1), brainstem (n=1), and cerebellopontine angle (n=1) (Figure 10A). No significant association of tumor location with patient age at diagnosis was apparent (Figure 10B). Kaplan-Meier analysis of overall survival in the 24 patients with available data revealed a poor prognosis in general, although the number of cases with adequate follow-up remains limited (Figure 10C).

Discussion

HGNET *BCOR* ex15 ITD is a recently proposed tumor entity of the central nervous system for which the clinicopathologic features have yet to be fully defined. Here, we have performed comprehensive clinicopathologic, radiographic, and genomic studies on a cohort of ten new cases. Together with the previously reported 25 cases in the scientific literature to date, our study better defines the distinctive radiographic and pathologic features that characterize this tumor entity, as well as providing detailed outcome data for children treated following either high-grade glioma or CNS embryonal tumor therapy protocols.

HGNET *BCOR* ex15 ITD usually presents as a large, well-circumscribed, heterogeneous mass with reduced diffusion and variable enhancement in the cerebral or cerebellar hemispheres. The majority arise in children younger than 5 years of age, but multiple cases in teenagers or young adults have now been observed. No sex predilection is apparent for this tumor entity, unlike other brain tumors entities such as astroblastoma-like neuroepithelial tumors with *MN1* alteration that demonstrate a significant female predominance (26).

HGNET *BCOR* ex15 ITD can demonstrate a wide morphologic spectrum, but usually feature a distinctive set of histologic and immunohistochemical features that provide clues to the diagnosis prior to molecular testing. Common features are a mostly solid growth pattern, GFAP-negative perivascular pseudorosettes, and monotonous round to ovoid nuclei with fine chromatin. Also, the characteristic combination of palisading necrosis without microvascular proliferation is helpful to differentiate these tumors from glioblastoma. The tumors can resemble anaplastic ependymomas due to perivascular pseudorosettes, astroblastomas due to perivascular pseudorosettes and hyalinized/collagenous stroma, or diffuse gliomas due to glial-like fibrillarity and infiltrative areas at their periphery. Those that contain structures resembling Homer Wright rosettes may also mimic medulloblastoma or CNS neuroblastoma, but differ from these entities based on their lack of synaptophysin expression. These are some of the most likely diagnoses that HGNET *BCOR* ex15 ITD may have received in the past. However, HGNET *BCOR* ex15 ITD have an unusual immunohistochemical profile with dual OLIG2 and NeuN positivity, along with sparse to absent GFAP expression and no synaptophysin expression, that can be helpful in distinguishing these tumors from potential histologic mimics. For example, this pattern is distinct from anaplastic ependymomas (usually OLIG2 negative, GFAP positive, and EMA positive with paranuclear dot-like staining), astroblastomas (usually GFAP positive), and diffuse gliomas (usually GFAP positive and NeuN negative). Additionally, the strong nuclear positivity for BCOR in virtually all tumor cells may be another helpful clue. However, the specificity of diffuse strong nuclear BCOR expression for this tumor entity needs to be further evaluated. For example, the pediatric low-grade gliomas with *EP300-BCOR* fusion can also demonstrate diffuse strong nuclear BCOR expression (27), and we have observed diffuse strong nuclear BCOR expression in an astroblastoma-like neuroepithelial tumor with *MN1* rearrangement that lacked *BCOR* exon 15 ITD (data not shown).

We believe these HGNET *BCOR* ex15 ITD are almost certainly of neuroepithelial origin (and therefore not sarcomas), based on the combination of their intraparenchymal location

within the brain, glioma-like fibrillarity, expression of OLIG2 and NeuN proteins, and absence of appreciable intercellular basement membrane deposition in most cases. While the identical *BCOR* exon 15 ITD is also present in two sarcoma entities, this most likely reflects a common molecular pathogenesis arising in distinct cells of origin: neural progenitor cell for HGNET *BCOR* ex15 ITD versus a mesenchymal progenitor cell for clear cell sarcoma of the kidney and primitive myxoid mesenchymal tumor of infancy. Future comparison of the genome-wide methylation and transcriptome profiles between the different tumor entities that all share the identical *BCOR* exon 15 ITD is likely to be informative in this regard.

While optimal treatment strategies remain uncertain for this tumor entity, the clinical data from this cohort do provide some new valuable insight. For instance, the one patient (SF-BCOR-4) in this cohort who did not receive any adjuvant radiation or chemotherapy after gross total resection experienced rapid local recurrence and also subsequently cerebrospinal dissemination. In combination with the poor outcomes observed for most patients to date, we believe that additional adjuvant therapy beyond the maximal safest resection possible should be strongly considered in all patients. Among the three children in our cohort that were treated following a high-grade glioma therapy protocol with cranial radiation and adjuvant temozolomide plus bevacizumab, two experienced local recurrence within 4 years after initial resection, whereas the third patient remains recurrence-free at approximately 2 years after initial resection. Among the six children in our cohort that were treated following a CNS embryonal tumor therapy protocol with intensive platinum-based chemotherapy regimens (three without radiation due to young patient age and three with cranial or craniospinal radiation), only one child experienced local recurrence at 14 months but is a long-term survivor who is currently alive without evidence of disease at 14 years after initial diagnosis. However, the follow-up interval is less than 2 years for the other five children, making the efficacy of this CNS embryonal tumor therapy protocol inconclusive at this point.

The high-grade neuroepithelial tumors in this cohort are all unified by the presence of an internal tandem duplication within exon 15 of the *BCOR* gene. This recurrent internal tandem duplication that is heterozygous (*i.e.* without loss of the remaining wildtype allele) and localizes within exon 15 that encodes the BCORL-PCGF1-binding domain is very likely to function as an activating, gain-of-function event. However, the specific mechanism by which this recurrent internal tandem duplication event in *BCOR* drives tumor development remains unknown, as are methods to therapeutically intervene using a precision medicine approach for these aggressive malignancies of childhood driven by *BCOR* exon 15 ITD.

Recent genomic investigation has revealed that distinct alterations in the *BCOR* gene are selected for in different brain tumor entities. Unlike the high-grade neuroepithelial tumors in this cohort defined by *BCOR* exon 15 ITD, a group of children with low-grade gliomas harboring in-frame *EP300-BCOR* gene fusions were recently reported that had divergent histologic features and a distinct genome-wide methylation profile compared to HGNET *BCOR* ex15 ITD (27). These gliomas with *EP300-BCOR* fusions had histologic features somewhat resembling either pilocytic astrocytoma or dysembryoplastic neuroepithelial tumor and lacked the perivascular pseudorosettes and palisading necrosis that characterize HGNET *BCOR* ex15 ITD. Additionally, truncating mutations or homozygous deletions of

BCOR or its homolog *BCORL1* have been recurrently found in retinoblastoma, medulloblastoma, and diffuse gliomas (12, 14, 16, 22, 29). Among diffuse gliomas, truncating mutations or homozygous deletions in the *BCOR* or *BCORL1* genes are present in a significant fraction of H3 K27M-mutant diffuse midline gliomas, as well as high-grade gliomas in the cerebral hemispheres of children (14, 29). In contrast to the exon 15 internal tandem duplication and in-frame fusion with *EP300* that are likely activating gain-of-function events, these recurrent nonsense or frameshift mutations as well as homozygous deletions in diffuse gliomas, medulloblastomas, and retinoblastomas are almost certainly functionally inactivating events. Thus, the oncogenic mechanisms by which *BCOR* alterations promote tumorigenesis are likely to be divergent dependent on the specific genetic alteration present. While Sturm *et al* initially proposed the terminology "CNS high-grade neuroepithelial tumor with *BCOR* alteration", it is now clear that the described entity was limited to those neuroepithelial tumors with exon 15 ITD and not merely any *BCOR* alteration (26). We thus recommend the more precise terminology of "CNS high-grade neuroepithelial tumor with *BCOR* exon 15 internal tandem duplication" for this tumor entity moving forward.

While the majority of cases in this patient cohort harbored *BCOR* exon 15 internal tandem duplication as the solitary pathogenic alteration, a subset harbored additional genetic alterations likely contributing to tumor pathogenesis. These were most frequently inactivating mutations within other transcriptional or epigenetic regulatory genes, including *EP300*, *SMARCA2*, *STAG2*, and *BCORL1*. Why these tumors selected for additional genetic alterations predicted to disrupt gene expression profiles beyond the *BCOR* exon 15 ITD is uncertain. Additionally, two of the cases contained *TERT* alterations, one with gene amplification and one with promoter hotspot mutation, indicating that telomere maintenance in a subset of HGNET *BCOR* ex15 ITD is accomplished by *TERT* activation. However, none of the ten cases harbored *ATRX* mutation or deletion, indicating that the alternative lengthening of telomeres typical of IDH-mutant and histone H3-mutant diffuse gliomas is not common in HGNET *BCOR* ex15 ITD.

Notably, none of the cases contained *IDH1* p.R132 or *IDH2* p.R172 mutations that define diffuse lower-grade gliomas in the cerebral hemispheres of adults (4). None of the cases contained *H3F3A* or *HIST1H3B* p.K27M mutation that define the majority of diffuse gliomas within midline structures of the CNS (14, 29). *H3F3A* p.G34 mutation or *SETD2* truncating mutation that define a subset of high-grade gliomas in the cerebral hemispheres of teenagers and young adults were not present in any of the cases (7, 14). No cases contained amplification, mutation, or rearrangement of receptor tyrosine kinase genes such as *EGFR*, *PDGFRA*, *MET*, *FGFR1–3*, *NTRK1–3*, *ALK*, or *ROS1* that are common in high-grade gliomas in children and adults (3, 14, 29). None of the cases contained *BRAF* mutation or rearrangement, nor any other alteration in components of the Ras-Raf-MAP kinase signaling pathway that are common in pediatric low-grade gliomas (31). None of the cases contained alterations in components of the PI3-kinase-Akt-mTOR signaling pathway including the *PTEN*, *TSC1*, *TSC2*, *PIK3CA*, or *PIK3R1* genes that are common in multiple glioma subtypes (3, 14, 31). *MYB* or *MYBL1* rearrangements that are common in pediatric low-grade gliomas were not found in any of the cases (31). None of the cases contained *MYC* or *MYCN* amplification that are common in Group 3 and 4 medulloblastomas, as well as a

subset of pediatric glioblastomas (14, 16). Additionally, none of the cases contained *RELA* or *YAP1* fusions or *NF2* mutation that are common in ependymomas (17). None of the cases contained *SMARCB1* or *SMARCA4* biallelic inactivation that defines atypical teratoid/rhabdoid tumor, although one tumor did harbor a heterozygous truncating mutation in the related *SMARCA2* chromatin remodeling gene. Thus, HGNET *BCOR* ex15 ITD appear to be genetically distinct from all other CNS tumor entities that have been molecularly defined to date.

In summary, we have comprehensively characterized the new tumor entity "High-grade neuroepithelial tumor with *BCOR* exon 15 internal tandem duplication". While the *BCOR* exon 15 ITD appears to be the solitary genetic driver in most cases, a subset also acquires additional genetic alterations that include *TERT* activation, *CDKN2A* homozygous deletion, and inactivating mutations in other transcriptional and epigenetic regulatory genes including *EP300*, *SMARCA2*, *STAG2*, and *BCORL1*. Rare examples may also acquire *TP53* mutational inactivation along with numerous chromosomal gains/losses that corresponds with histologic anaplasia. Future studies are warranted to identify the cellular mechanisms by which *BCOR* exon 15 ITD drives tumorigenesis and determine the optimal treatment strategies for affected children.

Supplementary Material

Refer to Web version on PubMed Central for supplementary material.

Acknowledgements

This study was supported by the NIH Director's Early Independence Award (DP5 OD021403) to D.A.S. We thank the staff of the UCSF Clinical Cancer Genomics Laboratory for assistance with genetic profiling. We thank the staff of the UCSF Electron Microscopy Core Lab (Cosima Carnahan and Sherry Kamiya) for assistance with ultrastructural analysis. We thank Sarah Bowman and Torrick Taylor for assistance with digital slide scanning.

REFERENCES

1. Appay R, Macagno N, Padovani L, Korshunov A, Kool M, Andre N et al. (2017) HGNET-BCOR tumors of the cerebellum: clinicopathologic and molecular characterization of 3 cases. Am J Surg Pathol 41:1254–1260. [PubMed: 28704208]
2. Astolfi A, Melchionda F, Perotti D, Fois M, Indio V, Urbini M et al. (2015) Whole transcriptome sequencing identifies BCOR internal tandem duplication as a common feature of clear cell sarcoma of the kidney. Oncotarget 6:40934–40939. [PubMed: 26516930]
3. Brennan CW, Verhaak RG, McKenna A, Campos B, Noushmehr H, Salama SR et al. (2013) The somatic genomic landscape of glioblastoma. Cell 155:462–477. [PubMed: 24120142]
4. Cancer Genome Atlas Research Network, Brat DJ, Verhaak RG, Aldape KD, Yung WK, Salama SR et al. (2015) Comprehensive, integrative genomic analysis of diffuse lower-grade gliomas. N Engl J Med 372:2481–2498. [PubMed: 26061751]
5. Damm F, Chesnais V, Nagata Y, Yoshida K, Scourzic L, Okuno Y et al. (2013) BCOR and BCORL1 mutations in myelodysplastic syndromes and related disorders. Blood 122:3169–3177. [PubMed: 24047651]
6. Fan Z, Yamaza T, Lee JS, Yu J, Wang S, Fan G et al. (2009) BCOR regulates mesenchymal stem cell function by epigenetic mechanisms. Nat Cell Biol 11:1002–1009. [PubMed: 19578371]
7. Fontebasso AM, Schwartzentruber J, Khuong-Quang DA, Liu XY, Sturm D, Korshunov A et al. (2013) Mutations in SETD2 and genes affecting histone H3K36 methylation target hemispheric high-grade gliomas. Acta Neuropathol 125:659–669. [PubMed: 23417712]

8. Grossmann V, Tiacci E, Holmes AB, Kohlmann A, Martelli MP, Kern W et al. (2011) Whole-exome sequencing identifies somatic mutations of BCOR in acute myeloid leukemia with normal karyotype. Blood 118:6153–6163. [PubMed: 22012066]

9. Huynh KD, Fischle W, Verdin E, Bardwell VJ (2000) BCoR, a novel corepressor involved in BCL-6 repression. Genes Dev 14:1810–1823. [PubMed: 10898795]

10. Kao YC, Sung YS, Zhang L, Huang SC, Argani P, Chung CT et al. (2016) Recurrent BCOR internal tandem duplication and YWHAE-NUTM2B fusions in soft tissue undifferentiated round cell sarcoma of infancy: overlapping genetic features with clear cell sarcoma of kidney. Am J Surg Pathol 40:1009–1020. [PubMed: 26945340]

11. Kline CN, Joseph NM, Grenert JP, van Ziffle J, Talevich E, Onodera C et al. (2017) Targeted next-generation sequencing of pediatric neuro-oncology patients improves diagnosis, identifies pathogenic germline mutations, and directs targeted therapy. Neuro-oncology 19:699–709. [PubMed: 28453743]

12. Kooi IE, Mol BM, Massink MP, Ameziane N, Meijers-Heijboer H, Dommering CJ et al. (2016) Somatic genomic alterations in retinoblastoma beyond RB1 are rare and limited to copy number changes. Sci Rep 6:25264. [PubMed: 27126562]

13. Lewis N, Soslow RA, Delair DF, Park KJ, Murali R, Hollmann TJ et al. (2018) ZC3H7B-BCOR high-grade endometrial stromal sarcomas: a report of 17 cases of a newly defined entity. Mod Pathol 31:674–684. [PubMed: 29192652]

14. Mackay A, Burford A, Carvalho D, Izquierdo E, Fazal-Salom J, Taylor KR et al. (2017) Integrated molecular meta-analysis of 1,000 pediatric high-grade and diffuse intrinsic pontine glioma. Cancer Cell 32:520–537. [PubMed: 28966033]

15. Ng D, Thakker N, Corcoran CM, Donnai D, Perveen R, Schneider A et al. (2004) Oculofaciocardiodental and Lenz microphthalmia syndromes result from distinct classes of mutations in BCOR. Nat Genet 36:411–416. [PubMed: 15004558]

16. Northcott PA, Buchhalter I, Morrissy AS, Hovestadt V, Weischenfeldt J, Ehrenberger T et al. (2017) The whole-genome landscape of medulloblastoma subtypes. Nature 547:311–317. [PubMed: 28726821]

17. Pajtler KW, Witt H, Sill M, Jones DT, Hovestadt V, Kratochwil F et al. (2015) Molecular classification of ependymal tumors across all CNS compartments, histopathological grades, and age groups. Cancer Cell 27:728–743. [PubMed: 25965575]

18. Panagopoulos I, Thorsen J, Gorunova L, Haugom L, Bjerkehagen B, Davidson B et al. (2013) Fusion of the ZC3H7B and BCOR genes in endometrial stromal sarcomas carrying an X;22-translocation. Genes Chromosomes Cancer 52:610–618. [PubMed: 23580382]

19. Paret C, Theruvath J, Russo A, Kron B, El Malki K, Lehmann N et al. (2016) Activation of the basal cell carcinoma pathway in a patient with CNS HGNET-BCOR diagnosis: consequences for personalized targeted therapy. Oncotarget 7:83378–83391. [PubMed: 27825128]

20. Peters TL, Kumar V, Polikepahad S, Lin FY, Sarabia SF, Liang Y et al. (2015) BCOR-CCNB3 fusions are frequent in undifferentiated sarcomas of male children. Mod Pathol 28:575–586. [PubMed: 25360585]

21. Pierron G, Tirode F, Lucchesi C, Reynaud S, Ballet S, Cohen-Gogo S et al. (2012) A new subtype of bone sarcoma defined by BCOR-CCNB3 gene fusion. Nat Genet 44:461–466. [PubMed: 22387997]

22. Pugh TJ, Weeraratne SD, Archer TC, Pomeranz Krummel DA, Auclair D, Bochicchio J et al. (2012) Medulloblastoma exome sequencing uncovers subtype-specific somatic mutations. Nature 488:106–110. [PubMed: 22820256]

23. Roy A, Kumar V, Zorman B, Fang E, Haines KM, Doddapaneni H et al. (2015) Recurrent internal tandem duplications of BCOR in clear cell sarcoma of the kidney. Nat Commun 6:8891. [PubMed: 26573325]

24. Santiago T, Clay MR, Allen SJ, Orr BA (2017) Recurrent BCOR internal tandem duplication and BCOR or BCL6 expression distinguish primitive myxoid mesenchymal tumor of infancy from congenital infantile fibrosarcoma. Mod Pathol 30:884–891. [PubMed: 28256570]

25. Specht K, Zhang L, Sung YS, Nucci M, Dry S, Vaiyapuri S et al. (2016) Novel BCOR-MAML3 and ZC3H7B-BCOR gene fusions in undifferentiated small blue round cell sarcomas. Am J Surg Pathol 40:433–442. [PubMed: 26752546]

26. Sturm D, Orr BA, Toprak UH, Hovestadt V, Jones DTW, Capper D et al. (2016) New brain tumor entities emerge from molecular classification of CNS-PNETs. Cell 164:1060–1072. [PubMed: 26919435]

27. Torre M, Meredith DM, Dubuc A, Solomon DA, Perry A, Vasudevaraja V, Serrano J, Snuderl M, Ligon KL, Alexandrescu S (2019) Recurrent EP300-BCOR fusions in pediatric gliomas with distinct clinicopathologic features. J Neuropathol Exp Neurol 78:305–314. [PubMed: 30816933]

28. Ueno-Yokohata H, Okita H, Nakasato K, Akimoto S, Hata J, Koshinaga T et al. (2015) Consistent in-frame internal tandem duplications of BCOR characterize clear cell sarcoma of the kidney. Nat Genet 47:861–863. [PubMed: 26098867]

29. Wu G, Diaz AK, Paugh BS, Rankin SL, Ju B, Li Y et al. (2014) The genomic landscape of diffuse intrinsic pontine glioma and pediatric non-brainstem high-grade glioma. Nat Genet 46:444–450. [PubMed: 24705251]

30. Yoshida Y, Nobusawa S, Nakata S, Nakada M, Arakawa Y, Mineharu Y et al. (2018) CNS high-grade neuroepithelial tumor with BCOR internal tandem duplication: a comparison with its counterparts in the kidney and soft tissue. Brain Pathol 28:710–720. [PubMed: 29226988]

31. Zhang J, Wu G, Miller CP, Tatevossian RG, Dalton JD, Tang B et al. (2013) Whole-genome sequencing identifies genetic alterations in pediatric low-grade gliomas. Nat Genet 45:602–612. [PubMed: 23583981]

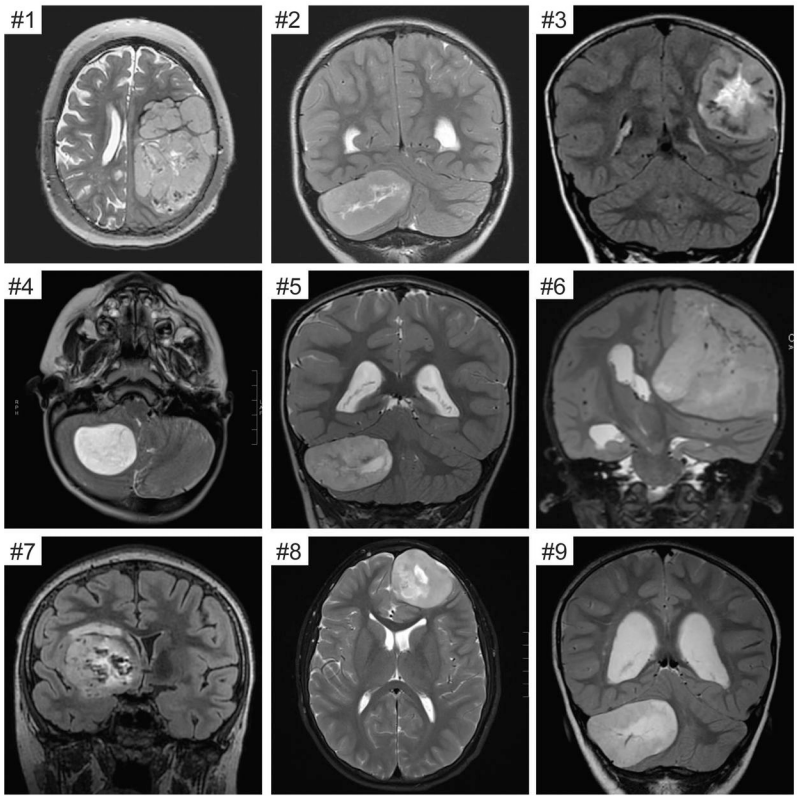

Figure 1. Imaging features of the CNS high-grade neuroepithelial tumors with BCOR exon 15 internal tandem duplication.

Shown are pre-operative magnetic resonance images for cases #1-9. All tumors were large, well-circumscribed, heterogeneous masses with variable enhancement and reduced diffusion. Many of the tumors demonstrated central areas of necrosis or blood products.

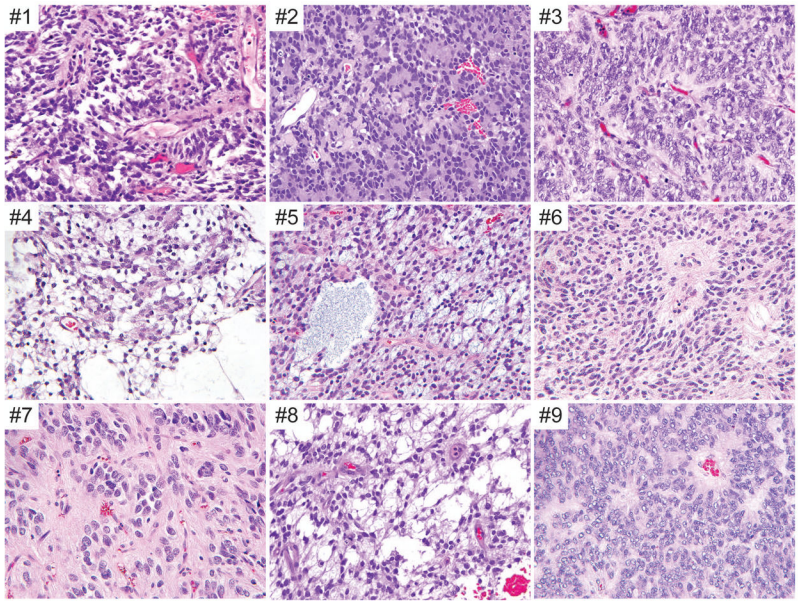

Figure 2. Histologic features of the CNS high-grade neuroepithelial tumors with BCOR exon 15 internal tandem duplication.

Shown are representative hematoxylin and eosin (H&E) stained sections of cases #1-9.

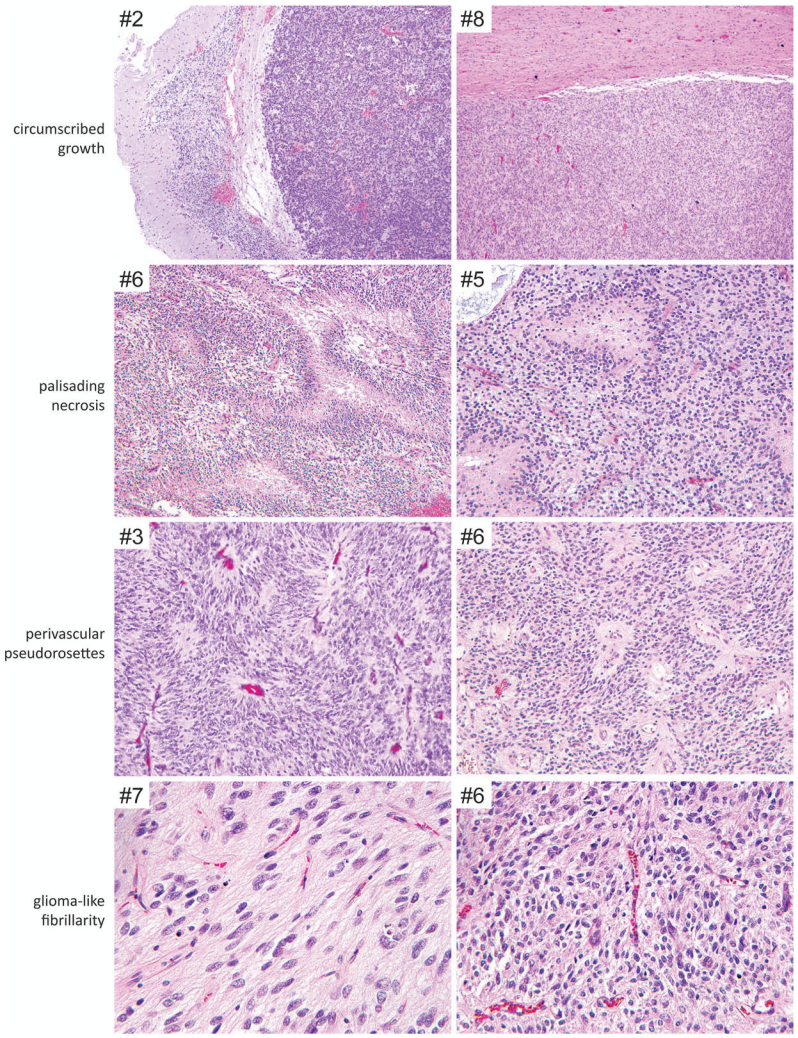

Figure 3. Recurrent histologic features observed in CNS high-grade neuroepithelial tumor with BCOR exon 15 internal tandem duplication.

Shown are H&E stained sections demonstrating the circumscribed growth, palisading necrosis, perivascular pseudorosettes, and glioma-like fibrillarity frequently observed in this tumor entity.

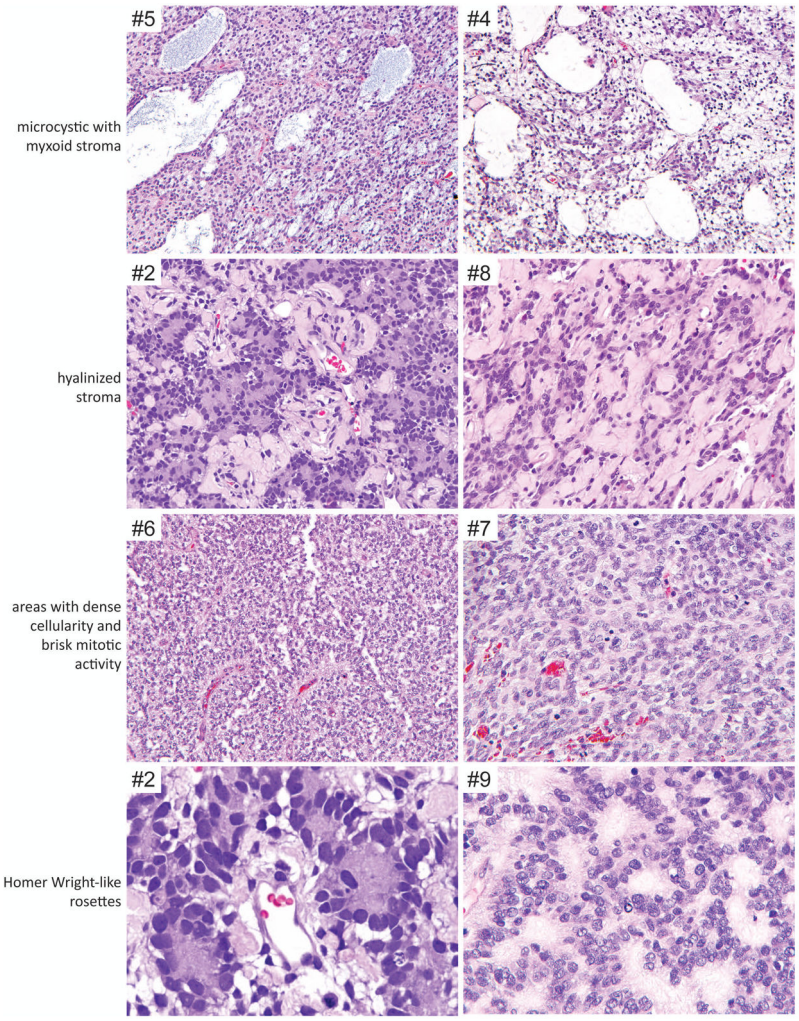

Figure 4. Additional recurrent histologic features observed in a subset of CNS high-grade neuroepithelial tumor with BCOR exon 15 internal tandem duplication.

Shown are H&E stained sections demonstrating the microcystic/myxoid background, hyalinized stroma, areas with dense cellularity and brisk mitotic activity, and Homer Wright-like rosettes observed in a subset of the cases.

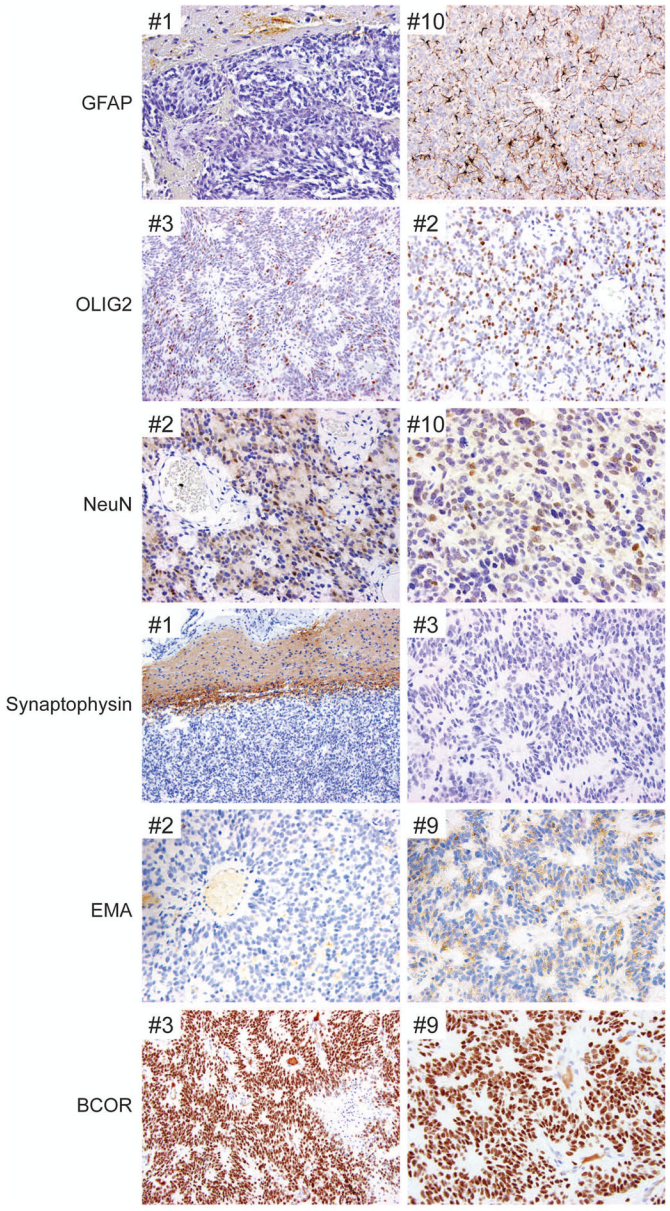

Figure 5. Immunohistochemical features of CNS high-grade neuroepithelial tumor with BCOR exon 15 internal tandem duplication.

Shown are representative immunohistochemical stains demonstrating the sparse to absent GFAP positivity, variable OLIG2 positivity, consistent NeuN positivity, synaptophysin negativity, granular cytoplasmic EMA staining with absence of paranuclear dot-like positivity, and diffuse strong nuclear BCOR expression.

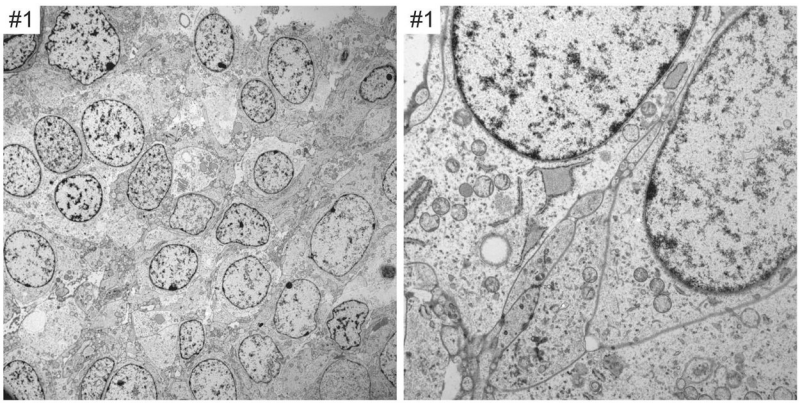

Figure 6. Ultrastructural features of CNS high-grade neuroepithelial tumor with BCOR exon 15 internal tandem duplication.

Shown are electron microscopy images demonstrating primitive cells with abundant rough endoplasmic reticulum. No tight junctions, cilia, or microvilli characteristic of ependymal differentiation are seen. Additionally, no neurosecretory granules or synaptic vesicles are observed.

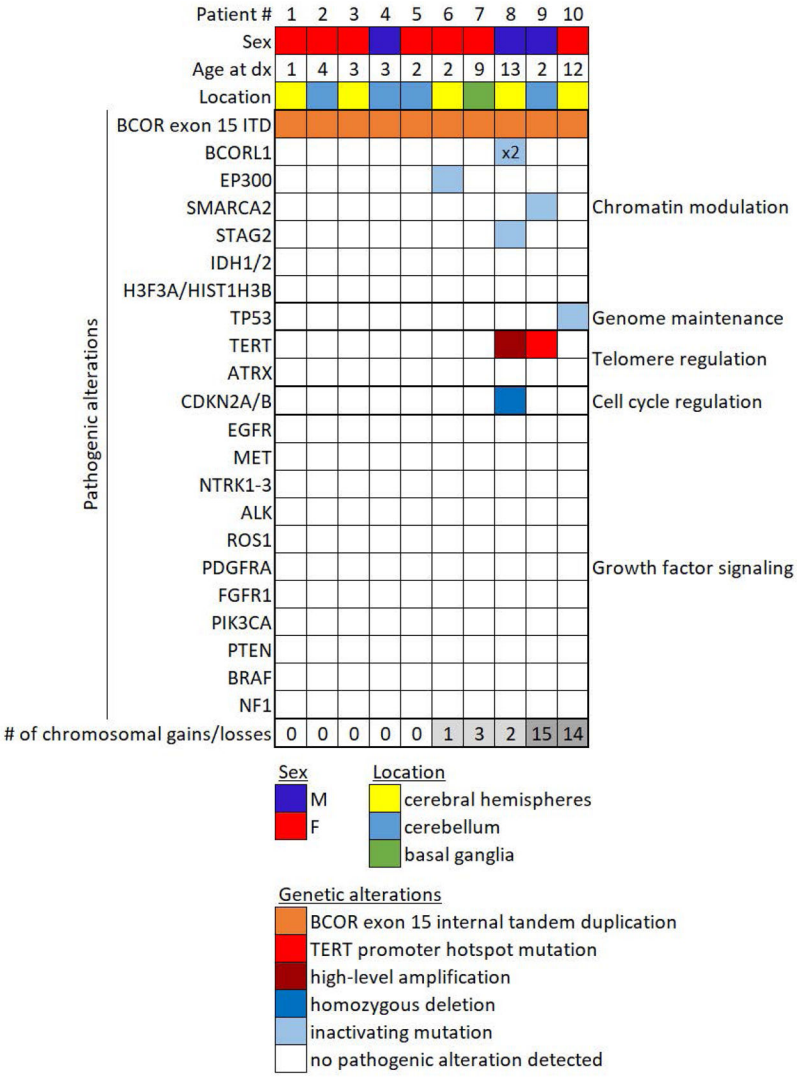

Figure 7. Genetic landscape of CNS high-grade neuroepithelial tumor with BCOR exon 15 internal tandem duplication.

Oncoprint table of the clinical features, likely pathogenic genetic alterations, and quantity of chromosomal copy number alterations in the ten cases.

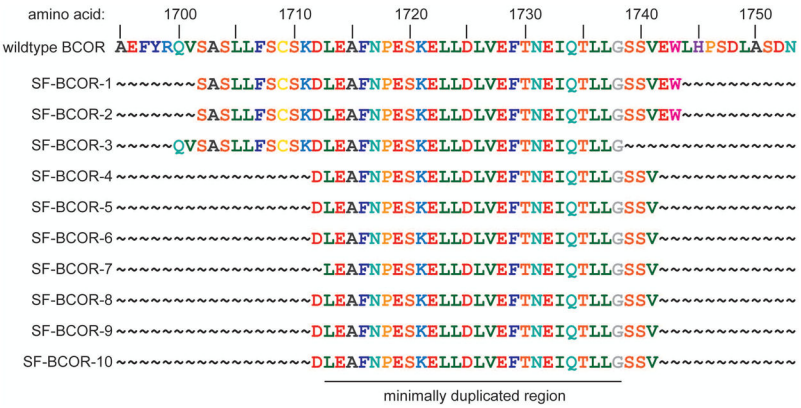

Figure 8.

Diagram of the amino acid sequence at the C-terminus of the BCOR protein showing the duplicated amino acids within exon 15 for the ten CNS high-grade neuroepithelial tumors with BCOR exon 15 internal tandem duplication.

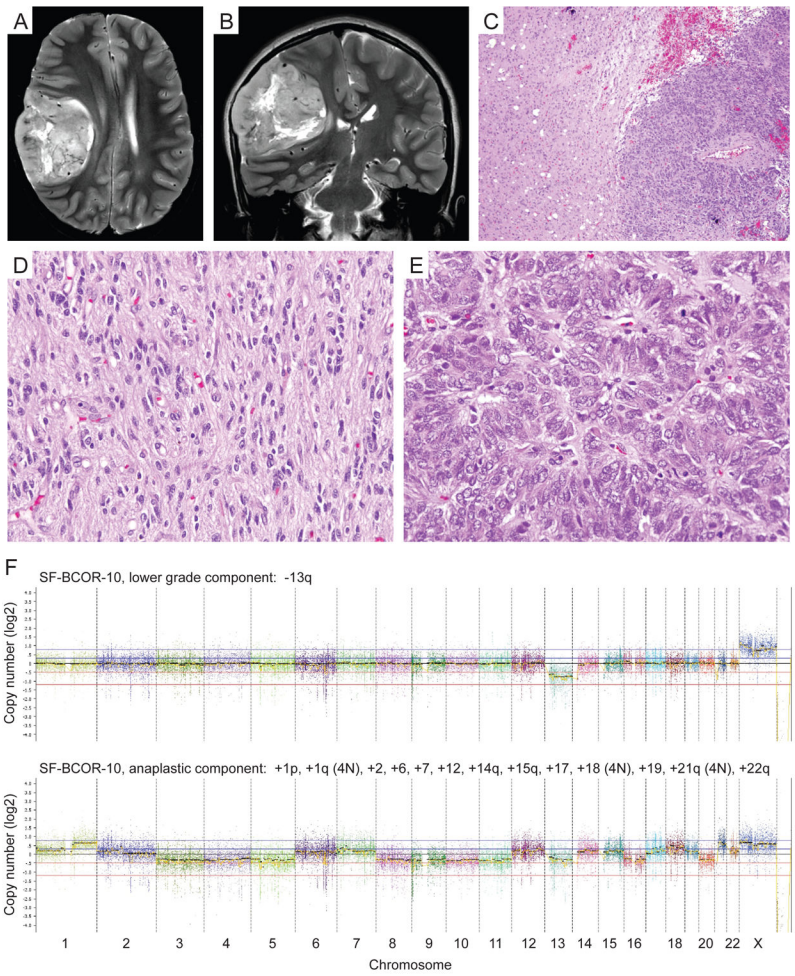

Figure 9. Anaplastic features in CNS HGNET BCOR ex15 ITD (case #10) in association with TP53 inactivation and marked aneuploidy.

A,B. Pre-operative axial and coronal T2-weighted MR images showing a circumscribed mass in the right cerebral hemisphere. **C,D,E.** H&E stained sections showing a biphasic tumor composed of a lower grade appearing component with abundant fibrillar processes (**C** left, **D**), and an anaplastic component with dense cellularity, severe nuclear pleomorphism, and brisk mitotic activity (**C** right, **E**). **F.** Genome-wide copy number plots for the lower grade appearing component showing monosomy 13q as the solitary copy number alteration (top), and for the anaplastic component showing numerous chromosomal gains and losses (bottom).

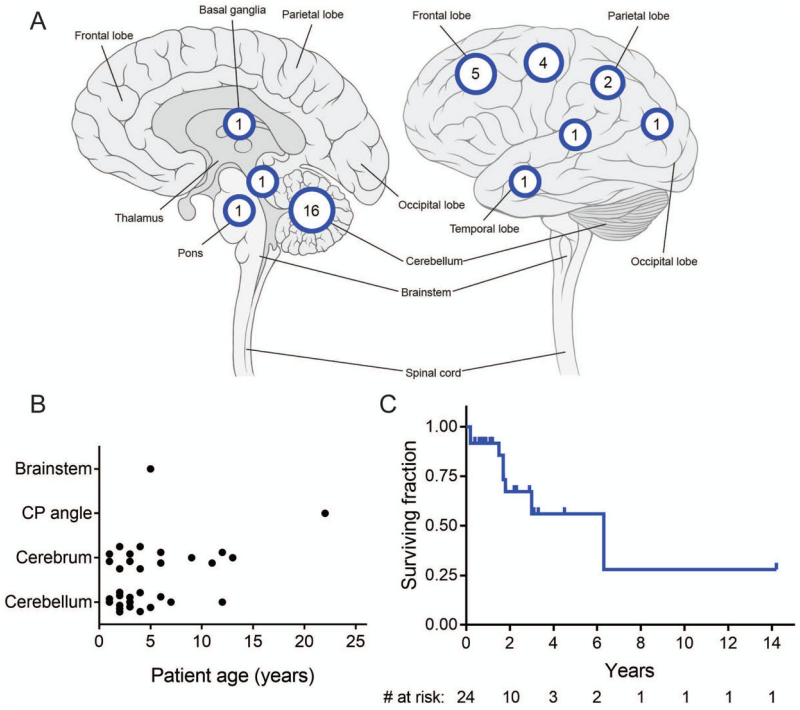

Figure 10. Clinical features of CNS high-grade neuroepithelial tumor with BCOR exon 15 internal tandem duplication.

Clinical data from the ten patients in this cohort (Supplementary Table 2), as well as all previously reported cases of this tumor entity with confirmed *BCOR* exon 15 internal tandem duplication (Supplementary Table 9), were aggregated for analysis. **A.** Location of the 33 tumors with specified anatomic site in the central nervous system. **B.** Age at initial diagnosis stratified by location for the 32 tumors with specified age and anatomic site. **C.** Kaplan-Meier survival analysis for the 24 patients with available clinical outcome data.

Table 1.

Clinical features of the ten patients with CNS high-grade neuroepithelial tumors with *BCOR* exon 15 internal tandem duplication.

Patient ID	Age (yrs)	Sex	Tumor location	Extent of resection	Radiation therapy	Initial chemotherapy	Recurrence	Follow-up (yrs)	Status at last follow-up
SF-BCOR-1	1	F	Frontoparietal lobe	GTR	None	Multiagent, platinum based	14 months	14.2	Alive, NED
SF-BCOR-2	4	F	Cerebellum	GTR	Craniospinal	Multiagent, platinum based	None	1.8	Alive, NED
SF-BCOR-3	3	F	Frontal lobe	GTR	Cranial	Multiagent, platinum based	None	0.4	Alive, NED
SF-BCOR-4	3	M	Cerebellum	GTR	None	None	4 months	2.3	Alive w/ disseminated disease
SF-BCOR-5	2	F	Cerebellum	GTR	None	Multiagent, platinum based	None	0.7	Alive, NED
SF-BCOR-6	2	F	Frontoparietal lobe	GTR	None	Multiagent, platinum based	None	0.8	Alive, NED
SF-BCOR-7	9	F	Basal ganglia	GTR	Cranial	Temozolomide & bevacizumab	None	2.2	Alive, NED
SF-BCOR-8	13	M	Frontal lobe	GTR	Cranial	Temozolomide & bevacizumab	49 months	4.5	Alive, NED
SF-BCOR-9	2	M	Cerebellum	GTR	Cranial	Temozolomide & bevacizumab	31 months	2.9	Alive, NED
SF-BCOR-10	12	F	Frontoparietal lobe	GTR	Craniospinal	Multiagent, platinum based	None	1.1	Alive, NED

Table 2.

Histologic features of the ten CNS high-grade neuroepithelial tumors with *BCOR* exon 15 internal tandem duplication.

Tumor ID	Growth pattern	Perivascular pseudorosettes	Homer Wright-like rosettes	Collagenous stroma	Myxoid/microcystic areas	Necrosis	Microvascular proliferation
SF-BCOR-1	Mostly solid	Present	Absent	Absent	Absent	Palisading	Absent
SF-BCOR-2	Solid	Present	Present	Present	Absent	Palisading	Absent
SF-BCOR-3	Solid	Present	Absent	Absent	Absent	Palisading	Absent
SF-BCOR-4	Solid	Present	Present	Absent	Present	Palisading	Absent
SF-BCOR-5	Mostly solid	Present	Absent	Absent	Present	Palisading	Absent
SF-BCOR-6	Solid	Present	Absent	Present	Present	Palisading	Absent
SF-BCOR-7	Solid	Present	Absent	Absent	Absent	Non-palisading	Absent
SF-BCOR-8	Solid and infiltrative	Present	Absent	Present	Present	Palisading	Absent
SF-BCOR-9	Solid	Present	Present	Absent	Present	Palisading	Absent
SF-BCOR-10	Solid and infiltrative	Present	Absent	Present	Absent	Palisading	Absent

Table 3.

Immunohistochemical features of the ten CNS high-grade neuroepithelial tumors with *BCOR* exon 15 internal tandem duplication.

Tumor ID	GFAP	OLIG2	NeuN	Synaptophysin	Neurofilament	EMA	p53	Ki-67	BCOR
SF-BCOR-1	negative	--	--	negative	positive (10%)	--	5%	20%	strongly positive
SF-BCOR-2	negative	positive (20%)	positive (10%)	negative	positive (10%)	granular cytoplasmic positivity	30%	--	--
SF-BCOR-3	negative	positive (20%)	negative	negative	positive (5%)	granular cytoplasmic positivity	--	40%	strongly positive
SF-BCOR-4	negative	positive (10%)	positive	negative	--	negative	15%	20%	--
SF-BCOR-5	focally positive	--	positive	negative	negative	negative	10%	15%	strongly positive
SF-BCOR-6	negative	--	positive (40%)	negative	positive (1%)	negative	10%	60%	strongly positive
SF-BCOR-7	negative	positive (30%)	positive (80%)	--	negative	negative	--	--	strongly positive
SF-BCOR-8	--	positive (40%)	positive (70%)	negative	negative	--	--	--	strongly positive
SF-BCOR-9	negative	negative	positive (20%)	negative	positive (10%)	granular cytoplasmic positivity	--	--	strongly positive
SF-BCOR-10 (LG)	negative	positive (20%)	positive (80%)	negative	negative	granular cytoplasmic positivity	0%	5%	strongly positive
SF-BCOR-10 (HG)	focally positive	negative	positive (20%)	negative	positive (1%)	granular cytoplasmic positivity	90%	60%	strongly positive

(LG), low-grade appearing component. (HG), high-grade/anaplastic component.

Table 4.

Genetic alterations in the ten CNS high-grade neuroepithelial tumors with *BCOR* exon 15 internal tandem duplication.

Tumor ID	*BCOR* exon 15 duplicated amino acids	Additional likely pathogenic alterations	Cytogenetic alterations
SF-BCOR-1	p.S1702_W1743	none	none
SF-BCOR-2	p.S1702_W1743	none	none
SF-BCOR-3	p.Q1700_G1738	none	none
SF-BCOR-4	p.D1712_V1741	none	none
SF-BCOR-5	p.D1712_V1741	none	none
SF-BCOR-6	p.D1712_V1741	*EP300* frameshift mutation	−18
SF-BCOR-7	p.L1713_V1741	none	+2p, −2q, −10
SF-BCOR-8	p.D1712_V1741	*BCORL1* frameshift mutation x2, *STAG2* splice site mutation, *TERT* promoter hotspot mutation, *CDKN2A/B* homozygous deletion	−9, −interstitial 10q
SF-BCOR-9	p.D1712_V1741	*SMARCA2* splice site mutation, *TERT* amplification	−distal 1p, +interstitial 1p, +1q, +2q, +interstitial 3q, +5p, +proximal 5q, +7, −9p, +12, −distal 14q, −proximal 15q, +20
SF-BCOR-10	p.D1712_V1741	*TP53* missense mutation	+1p, +1q, +2, +6, +7, +12, +14q, +15q, +17, +18, +19, +21q, +22q